Am J Nucl Med Mol Imaging 2015;5(1):38-45
www.ajnmmi.us /ISSN:2160-8407/ajnmmi0002503

Original Article

Simultaneous hyperpolarized ^{13}C-pyruvate MRI and ^{18}F-FDG-PET in cancer (hyperPET): feasibility of a new imaging concept using a clinical PET/MRI scanner

Henrik Gutte[1,2*], Adam E Hansen[1*], Sarah T Henriksen[1,3], Helle H Johannesen[1], Jan Ardenkjaer-Larsen[3,4], Alexandre Vignaud[5], Anders E Hansen[2,6], Betina Børresen[7], Thomas L Klausen[1], Anne-Mette N Wittekind[1], Nic Gillings[1], Annemarie T Kristensen[7], Andreas Clemmensen[1,2], Liselotte Højgaard[1], Andreas Kjær[1,2]

[1]Department of Clinical Physiology, Nuclear Medicine and PET, Rigshospitalet, University of Copenhagen, Denmark; [2]Cluster for Molecular Imaging, Faculty of Health Sciences, University of Copenhagen, Denmark; [3]Department of Electrical Engineering, Technical University of Denmark, Lyngby, Denmark; [4]GE Healthcare, Brøndby, Denmark; [5]CEA Saclay, I2BM, NeuroSpin, UNIRS, Gif sur Yvette, France; [6]Center for Nanomedicine and Theranostics, Technical University of Denmark, Denmark; [7]Department of Veterinary Clinical and Animal Sciences, Faculty of Health and Medical Sciences, University of Copenhagen, Frederiksberg C, Denmark. [*]Equal contributors.

Received September 14, 2014; Accepted September 29, 2014; Epub December 15, 2014; Published January 1, 2015

Abstract: In this paper we demonstrate, for the first time, the feasibility of a new imaging concept - combined hyperpolarized ^{13}C-pyruvate magnetic resonance spectroscopic imaging (MRSI) and ^{18}F-FDG-PET imaging. This procedure was performed in a clinical PET/MRI scanner with a canine cancer patient. We have named this concept *hyper PET*. Intravenous injection of the hyperpolarized ^{13}C-pyruvate results in an increase of ^{13}C-lactate, ^{13}C-alanine and ^{13}C-CO_2 (^{13}C-HCO_3) resonance peaks relative to the tissue, disease and the metabolic state probed. Accordingly, with dynamic nuclear polarization (DNP) and use of ^{13}C-pyruvate it is now possible to directly study the *Warburg Effect* through the rate of conversion of ^{13}C-pyruvate to ^{13}C-lactate. In this study, we combined it with ^{18}F-FDG-PET that studies uptake of glucose in the cells. A canine cancer patient with a histology verified local recurrence of a liposarcoma on the right forepaw was imaged using a combined PET/MR clinical scanner. PET was performed as a single-bed, 10 min acquisition, 107 min post injection of 310 MBq ^{18}F-FDG. ^{13}C-chemical shift imaging (CSI) was performed just after FDG-PET and 30 s post injection of 23 mL hyperpolarized ^{13}C-pyruvate. Peak heights of ^{13}C-pyruvate and ^{13}C-lactate were quantified using a general linear model. Anatomic ^{1}H-MRI included axial and coronal T1 vibe, coronal T2-tse and axial T1-tse with fat saturation following gadolinium injection. In the tumor we found clearly increased ^{13}C-lactate production, which also corresponded to high ^{18}F-FDG uptake on PET. This is in agreement with the fact that glycolysis and production of lactate are increased in tumor cells compared to normal cells. Yet, *most interestingly,* also in the muscle of the forepaw of the dog high ^{18}F-FDG uptake was observed. This was due to activity in these muscles prior to anesthesia, which was *not* accompanied by a similarly high ^{13}C-lactate production. Accordingly, this clearly demonstrates how the *Warburg Effect* directly can be demonstrated by hyperpolarized ^{13}C-pyruvate MRSI. This was not possible with ^{18}F-FDG-PET imaging due to inability to discriminate between causes of increased glucose uptake. We propose that this new concept of simultaneous hyperpolarized ^{13}C-pyruvate MRSI and PET may be highly valuable for image-based non-invasive phenotyping of tumors. This methods may be useful for treatment planning and therapy monitoring.

Keywords: Cancer, DNP, hyperpolarized, ^{13}C-pyruvate, MR, response monitoring, ^{18}F-FDG-PET, PET/MR, molecular imaging

Introduction

Traditionally, staging and anti-cancer therapy monitoring has been performed by morphological imaging methods. CT imaging applying RECIST criteria or similar criteria, has been the standard method [1]. Where CT is of less sensitive, e.g. brain and prostate tumors, morphological proton MRI is largely applied [2, 3]. However, recently it has been acknowledged that imaging methods visualizing tumor phenotype may be of greater value [4, 5]. Especially visualization of metabolism, one of the hallmarks of cancer, has drawn attention as a most

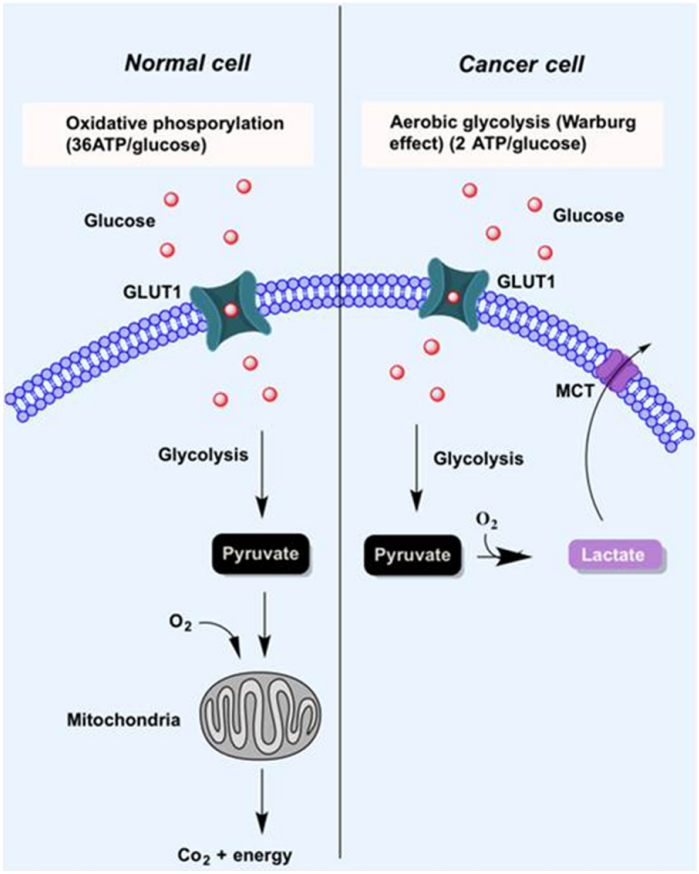

Figure 1. Schematic diagram illustrating the *Warburg effect* and the metabolic difference between cancer and normal non-hypoxic cells. Normal cells primarily rely on mitochondrial oxidative phosphorylation to generate the energy needed for the cellular processes. In contrast, most cancer cells are switched to aerobic glycolysis, even in the presence of oxygen, the *Warburg effect*. Accordingly in cancer cells most glucose when metabolized to pyruvate will be further converted into lactate even in the presence of oxygen. Since glucose metabolism in normal non-hypoxic cells through oxidative phosphorylation is much more effective than aerobic glycolysis, much higher amounts of glucose is utilized in cancer cells (10-20 fold) even if these cells do not have a higher energy need.

powerful tool to characterize solid tumors [6-8]. A key metabolic fingerprint in cancer cells is the switch to glycolysis with production of lactate even in the presence of sufficient oxygen [9-12], as illustrated in **Figure 1**. This phenomenon was first described by Heinrich Otto Warburg in 1924 and has since been named the *Warburg effect* [13, 14]. Since glucose metabolism in normal non-hypoxic cells through oxidative phosphorylation is much more efficient in ATP production than anaerobic glycolysis, higher amounts of glucose are utilized in cancer cells (10-20 fold) even if these cells do not have a higher energy need [4]. This high uptake forms the basis for visualizing cancer cells and tumors using the glucose analogue ^{18}F-2-fluoro-2-deoxy-D-glucose (^{18}F-FDG) [6, 8]. ^{18}F-FDG is transported into the cells by the same systems as glucose, i.e. GLUT transporters. However, in contrast to glucose, once ^{18}F-FDG is phosphorylated by hexokinases it is not further metabolized and thus trapped in the cells [9, 11]. In agreement with this, it has been shown in numerous studies that ^{18}F-FDG accumulation correlates with prognosis [15, 16] and has proven its value in management of many types of cancer patients [17]. However, it should be noted that ^{18}F-FDG uptake is only an indirect measure of the *Warburg Effect*. Accordingly, non-cancer tissue with high glucose consumption and subsequent oxidative phosphorylation will also present with high ^{18}F-FDG uptake and accumulation, e.g. working muscles, inflammation, and in the highly metabolic active brain. Finally, in all cells with high proliferative rates an increased uptake of ^{18}F-FDG is seen.

To further characterize tumors phenotypically, methods specifically looking at the metabolic pathways are of value. Magnetic Resonance Spectroscopy (MRS) is a technique that offers non-invasive *in vivo* assessment of tissue chemistry and cellular metabolism [18]. However, the low sensitivity of MRS has largely limited its use for this. Recently, development of the technique of Dynamic Nuclear Polarization (DNP) circumvented this elegantly. DNP is capable of creating solutions of molecules with polarized nuclear spins in various nuclei and has enabled real-time investigation of *in vivo* metabolism. The development of this new method has enhanced the nuclear polarization more than 10,000-fold, thereby significantly increasing the sensitivity of MRS [19]. Furthermore, the method enables measuring the kinetics of the conversion of the substrate into other cell metabolites and can be combined with anatomical proton MRI. Different nuclei have been hyperpolarized

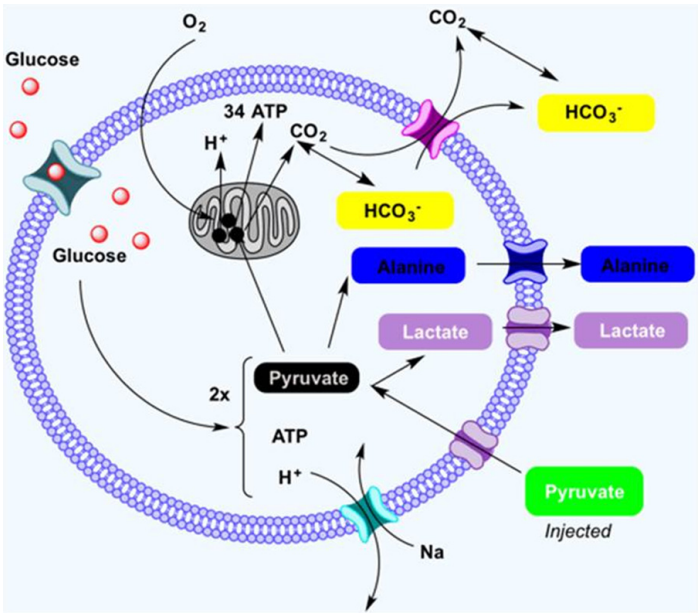

Figure 2. Simplistic illustration of the pyruvate cycle showing pyruvate converted from glucose through glycolysis. When oxygen is present pyruvate is transported to the mitochondria and undergoes oxidative phosphorylation with production of ATP, CO_2 and H^+. When oxygen is depleted (anaerobic glycolysis) or in cancer cells even in presence of oxygen (aerobic glycolysis) pyruvate is converted to lactate.

using the DNP method. Currently, the most widely used nucleus has been ^{13}C due to favoring characteristics and the possibility of incorporating ^{13}C into biologically relevant compounds, e.g. pyruvate. Intravenous injection of hyperpolarized ^{13}C-pyruvate results in the increase of ^{13}C-lactate, ^{13}C-alanine and ^{13}C-CO_2 (^{13}C-HCO_3) resonance peaks relative to the tissue, disease and the metabolic state probed [19, 20]. **Figure 2** illustrates the cell metabolism of ^{13}C-pyruvate. Accordingly, with DNP and use of ^{13}C-pyruvate it is now possible to directly study the *Warburg effect* through the rate of conversion from ^{13}C-pyruvate to ^{13}C-lactate [21, 22].

The aim of our study was therefore to demonstrate, for the first time, the feasibility of simultaneous *in vivo* PET combined with hyperpolarized MRI. Specifically, we aimed to show that ^{18}F-FDG-PET could be combined with ^{13}C-pyruvate magnetic resonance spectroscopic imaging (MRSI) for characterization of cancer using a clinical PET/MRI scanner.

Methods

A canine cancer patient (female Labrador Retriever, 32 kg) with a biopsy-verified local recurrence of a liposarcoma on the right ante brachium was the test subject. Imaging was performed using a combined PET/MR clinical scanner (Siemens mMR Biograph, Siemens, Erlangen, Germany). The liposarcoma had been irradiated two years prior to recurrence (4 fractions) and surgically removed. The dog was premedicated with Methadone (0.2 mg/kg IM) and anaesthetized using a bolus injection of Propofol. Anesthesia was maintained by a continuous intravenous infusion of Propofol (15-25 mg/kg/h). Heart rate, oxygen saturation, and blood pressure were measured throughout the scanning procedure. In the periphery of the lesion, fish oil capsules were placed for better delineation of the tumor on the localizers datasets. The dog was placed in prone position head-first. MRI utilized a dual tuned flex coil (RAPID Biomedical, Rimpar, Germany). A 5.5 mL vial of 4.0 M ^{13}C-urea mixed with Gadolinium (Dotarem, GUERBET, Roissy, France) at the back of the coil was used for MR flip angle calibration and frequency centering. The coil was placed above the front leg and centered on the lesion.

The study was approved by The Ethics and Administrative Committee, Department of Clinical Veterinary and Animal Sciences, Faculty of Health and Medical Sciences, University of Copenhagen.

Hyperpolarized ^{13}C-pyruvate

Hyperpolarized ^{13}C-pyruvate was prepared using the SpinLab system (GE Healthcare, Millwaukee, WI, USA). The ^{13}C-pyruvate sample consisted of [1-^{13}C]pyruvic acid mixed with an Electron Paramagnetic Agent (EPA) manufactured by Syncom (Groningen, Netherlands, PN AH111501. The EPA concentration in the sample is 15 mM. The dissolution media applied contains 0.1 g/L ethylenediaminetetraacetic acid disodium salt dehydrate (EDTA disodium salt, Sigma PN E4994) in water. The neutralization media used to neutralize the hyperpolarized [1-^{13}C]pyruvic acid sample prior to injection contains 0.72 M NaOH, 0.4 M Tris and 0.1 g/L EDTA disodium salt in water.

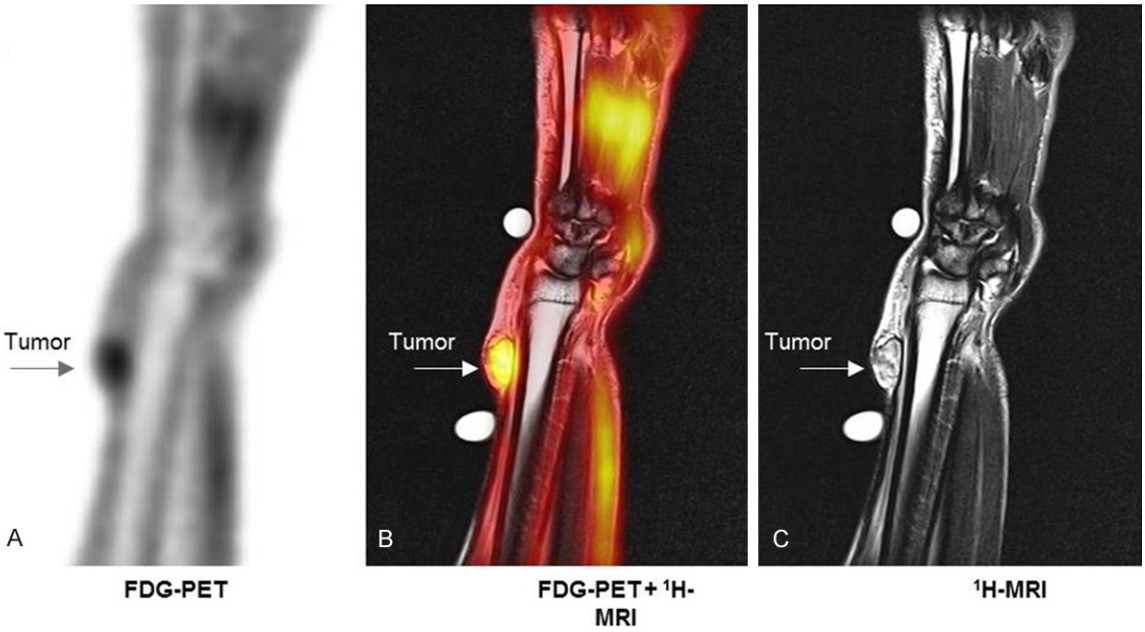

Figure 3. Coronal ^{18}F-FDG-PET/MR images of right front leg showing the liposarcoma (arrow). Note the high concentration of ^{18}F-FDG in the muscle. A: ^{18}F-FDG-PET. B: T2_TSE + ^{18}F-FDG-PET. C: T2_TSE.

^{1}H-MR-imaging

Localizer images and manual ^{13}C flip angle calibration was followed by anatomic ^{1}H-MRI, including axial T1 vibe and coronal T2-tse. In an axial-oblique 40 mm thick slab including the tumor region, dynamic ^{13}C-MRS was performed. Parameters were repetition time (TR) 1,000 ms, echo time (TE) 0.757 ms, flip angle 5°, bandwidth 4,000 Hz. The acquisition was repeated 180 times, commencing at the injection of the hyperpolarized ^{13}C-pyruvate (23 mL).

^{18}F-FDG imaging

PET was performed as a single-bed, 10 min acquisition, 107 min post iv injection of 310 MBq ^{18}F-FDG. Image reconstruction was performed using 3D OP-OSEM 4i21s, matrix 344, 4 mm Gaussian post-filter and vendor supplied attenuation correction algorithms.

^{13}C-chemical shift imaging

^{13}C-chemical shift imaging (CSI) was undertaken just after ^{18}F-FDG-PET and 30 s post injection of 23 mL hyperpolarized ^{13}C-pyruvate (250 mM). Parameters were repetition time 80 ms, flip angle 23°, bandwidth 10,000 Hz, FOV 80 mm, slice thickness 23 mm, matrix 16x16 (circular truncation) and total imaging time 11 s. The 30 s delay was chosen to obtain maximum ^{13}C-lactate signal during imaging based on the previous dynamic ^{13}C-MRS acquisition. Finally, axial T1-tse MRI with fat saturation was performed following gadolinium injection (6.4 mL Dotarem). Peak heights of ^{13}C-pyruvate, ^{13}C-actate, ^{13}C-alanine and ^{13}C-pyruvate hydrate were quantified using a general linear model implemented in Matlab (MathWorks, Natick, MA, USA). A set of additional components were included in the model to account for frequency shifts and peak splitting of the ^{13}C-pyruvate and ^{13}C-lactate peak observed in voxels containing vascular tissue. Further, the first and second derivatives of all metabolites were included in the model. The estimation was performed in the frequency domain on baseline corrected spectra. We report the ratio of ^{13}C-lactate normalized to the sum of all modeled peak heights.

Results

Work-flow

We found that combined FDG-PET and ^{13}C-pyruvate MRSI was feasible in a single session of approximately 2 h. A continuous work-flow was obtained with start of hyperpolarization of ^{13}C-pyruvate and injection of FDG-PET almost at the same time. After approximately 1½ h a

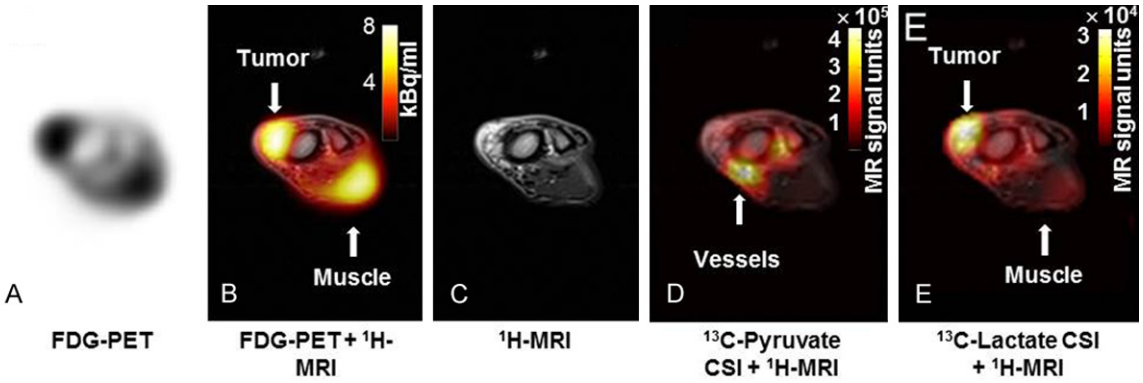

Figure 4. Transaxial images of right front leg showing the liposarcoma. Note the high concentration of ^{18}F-FDG in muscle (arrow, panel B, ^{18}F-FDG-PET + ^{1}H-MRI) and of ^{13}C-pyruvate in the large vessels (arrow in panel D, ^{13}C-Pyruvate CSI + ^{1}H-MRI). A: ^{18}F-FDG-PET. B: ^{18}F-FDG-PET + ^{1}H-MRI. C: ^{1}H-MRI. D: ^{13}C-Pyruvate CSI + ^{1}H-MRI. E: ^{13}C-lactate CSI + ^{1}H-MRI.

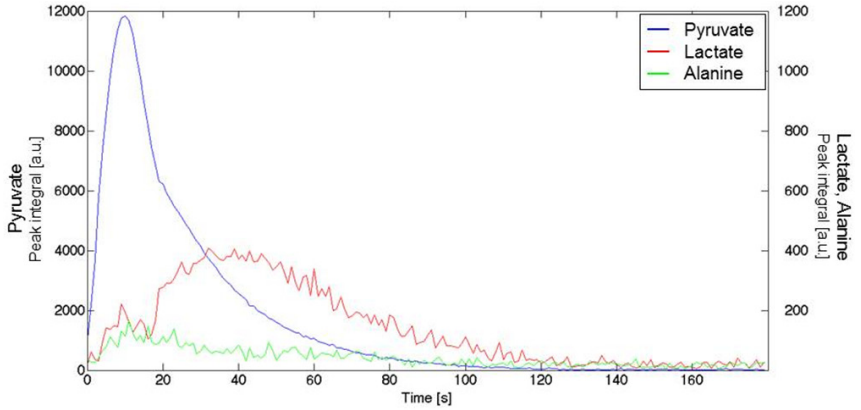

Figure 5. The dynamic ^{13}C-MRS showed initially a large peak 10 s after the injection of the ^{13}C-pyruvate. This was followed by generation of ^{13}C-lactate, with the peak concentration appearing approximately 40 s after injection.

10 min FDG-PET acquisition was performed that was immediately followed by dissolution and injection of ^{13}C-pyruvate that took less than 30 s in our setup. Acquisition of ^{13}C-lactate and ^{13}C-pyruvate spectra lasted less than 2 min. ^{1}H-MR-imaging was performed between FDG injection and FDG-PET acquisition.

^{1}H-MRI

The tumor was easily delineated on ^{1}H-MRI as clearly seen on the coronal images (**Figure 3**).

^{18}F-FDG imaging

On both coronal and transaxial images a high uptake of ^{18}F-FDG in the tumor (liposarcoma) was observed. Furthermore, also in muscles a clear uptake of ^{18}F-FDG was seen (**Figures 3** and **4**). Quantification of ^{18}F-FDG uptake in the tumor revealed a SUV_{max} of 1.52 the transaxial slice where ^{13}C-chemical shift imaging was performed (**Figure 4**). For muscle the SUV_{max} in the same slice was found to be almost as high, namely 1.26 (**Figure 4**).

^{13}C-chemical shift imaging (CSI)

Initially a dynamic ^{13}C-MRS was performed (**Figure 5**). The dynamic MRS showed a large peak 10 s after the injection of the ^{13}C-pyruvate. This initial peak was followed by generation of ^{13}C-lactate, with the peak concentration appearing approximately 30 to 40 s after ^{13}C-pyruvate injection (**Figure 5**). Comparatively, only very low levels of ^{13}C-alalnine were generated (**Figure 4**). For subsequent static CSI a delay of 30 s was therefore chosen relative to injection of ^{13}C-pyruvate to obtain imaging at the peak of lactate concentration. ^{13}C-pyruvate and ^{13}C-lactate CSI are shown in **Figure 4D** and **4E**, respectively. We observed high ^{13}C-pyruvate concentration in voxels encompassing the large vessels adjacent to the muscle corresponding to the injected ^{13}C-pyruvate (**Figure 4D**). In the CSI data sets, increased ^{13}C-lactate production

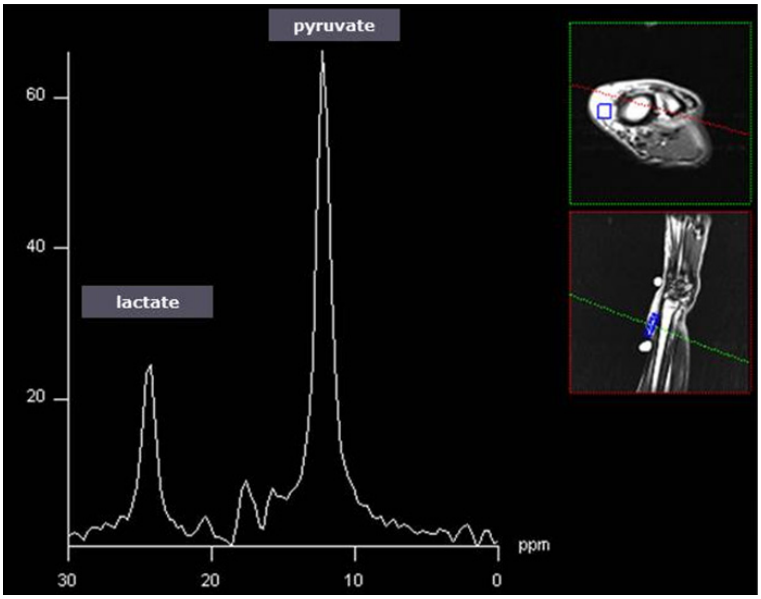

Figure 6. Single ^{13}C-CSI spectrum visualizing the ^{13}C-lactate and ^{13}C-pyruvate peaks in a voxel within the liposarcoma.

was observed in the tumor (**Figure 4E**). Calculation of the ^{13}C-lactate/^{13}C-pyruvate ratio revealed a ratio of 0.213 in the tumor, 0.078 in the muscle and 0.038 in the vasculature) (**Figure 4**). The tumor area with highest ^{13}C-lactate/^{13}C-pyruvate ratio also had the highest ^{18}F-FDG uptake. In **Figure 6** ^{13}C-MRS of a single voxel encompassed in the tumor is shown. Note that ^{13}C-lactate and ^{13}C-pyruvate are clearly seen as distinct peaks.

Discussion

To our knowledge this is the first study acquiring both ^{13}C-lactate/^{13}C-pyruvate CSI and ^{18}F-FDG-PET using a combined clinical PET/MR scanner. We found that this new concept, *hyperPET*, simultaneous hyperpolarized ^{13}C-pyruvate MRSI and ^{18}F-FDG-PET, is feasible and may be a highly valuable tool for image-based non-invasive phenotyping of tumors. In our study we were able to visualize in real time the *in vivo* metabolism of ^{13}C-pyruvate and conversion into ^{13}C-lactate in a spontaneous canine liposarcoma. In the tumor we found clearly ^{13}C-lactate production, which also corresponded to high ^{18}F-FDG uptake on PET. This is in agreement with the well-know fact that glycolysis and production of lactate are increased in tumor cells compared to normal cells [4]. However, *most interestingly* also in the muscle of the forepaw of the dog, high ^{18}F-FDG uptake was observed due to use of these muscles prior to anesthesia but this was *not* accompanied by a similarly high ^{13}C-lactate production. Accordingly, this clearly demonstrates how the *Warburg effect* is specifically shown by ^{13}C-pyruvate MRSI whereas ^{18}F-FDG was not capable of this and cannot discriminate between whether glucose uptake is increased due to oxidative phosphorylation operating at a high level or due to glycolysis.

In our study, we used a canine cancer patient with a spontaneous syngeneic cancer as it mirrors biological behavior of human cancer including heterogeneity, microenvironment, mode of progression, metastasis etc.. Accordingly, cancer bearing dogs represent a unique clinical cancer model with a direct potential for facilitating translation of results to human patients [23].

Technically, a simple CSI technique was employed for spectroscopic imaging in the current study. More advanced techniques allow for faster, volumetric and repeated spectroscopic imaging (for review, see [24, 25]). Such techniques therefore permit for larger spatial coverage and more detailed characterization of the tumor metabolism. We aim at implementing these techniques in future studies.

The use of hyperpolarized ^{13}C-pyruvate has previously in preclinical studies been shown to be a sensitive method for diagnosing cancer and assessment of early treatment response in a variety of cancers [26]. Recently, a first-in-man study of 31 patients was conducted with the primary objective to assess the safety of hyperpolarized ^{13}C-pyruvate in healthy subjects and prostate cancer patients. The study showed an elevated ^{13}C-lactate/^{13}C-pyruvate ratio in regions of biopsy-proven prostate cancer [27]. With the emergence of hybrid PET/MR systems and the present study demonstrating feasibility of *hyperPET*, we therefore suggest that combined ^{18}F-FDG-PET and ^{13}C-pyruvate MRSI could be valuable in the clinical work-up of cancer patients. MRS imaging with ^{13}C-pyruvate

may therefore have clinical relevance as added information when used together with ^{18}F-FDG-PET and provide better phenotyping of tumors. In addition, hyperpolarized ^{13}C-pyruvate MRS imaging may be the only feasible way to study glycolysis in tumors where ^{18}F-FDG-PET is of little value as in prostate cancer (low ^{18}F-FDG uptake and high bladder activity) and brain tumors (high physiological uptake in the brain).

With regard to early response monitoring in cancer treatment, the possibility exists that ^{13}C-pyruvate can detect such effects earlier than ^{18}F-FDG-PET. However, this remains to be answered through comparative PET and hyperpolarized MRSI studies. From both a clinical and basic science perspective, further comparison of PET and ^{13}C-pyruvate-lactate conversion is needed to elucidate the differential information gained from the modalities. Previous preclinical comparison studies have been carried out on separate systems [28, 29], with a potential error arising from the time difference between the examinations and errors in positioning of the animal. However, the introduction of integrated PET/MR systems allows for single-session, simultaneous MRI and PET. At present such combined studies with hyperpolarized MRSI and PET remains to be performed.

With the current study carried out on a canine cancer patient with a liposarcoma and using a clinical PET/MRI scanner we have clearly demonstrated that concurrent DNP ^{13}C-lactate/^{13}C-pyruvate CSI and ^{18}F-FDG-PET imaging is feasible in a clinical setting. Future, systematic studies are needed to assess the clinical value of combining these modalities within oncology.

Conclusion

To our knowledge this is first study acquiring both DNP ^{13}C-lactate/^{13}C-pyruvate CSI and ^{18}F-FDG-PET using a combined PET/MR scanner. We propose that this new concept of simultaneous hyperpolarized ^{13}C-imaging and ^{18}F-FDG-PET may be highly valuable for image-based non-invasive phenotyping of tumors. Translation into humans of this technique will demonstrate whether it is of clinical value.

Acknowledgements

The financial support from the John and Birthe Meyer Foundation and the Capital Region of Denmark is gratefully acknowledged. Karin Staehr, Marianne Federspiel, Jakup Poulsen and Betina Senius Pedersen are acknowledged for invaluable technical assistance.

Address correspondence to: Dr. Andreas Kjaer, Department of Clinical Physiology, Nuclear Medicine & PET, KF-4012, Rigshospitalet, National University Hospital, Blegdamsvej 9, DK-2100 Copenhagen, Denmark. Tel: + 45 3545 4011; Fax: + 45 3545 4015; E-mail: akjaer@sund.ku.dk

References

[1] Eisenhauer EA, Therasse P, Bogaerts J, Schwartz LH, Sargent D, Ford R, Dancey J, Arbuck S, Gwyther S, Mooney M, Rubinstein L, Shankar L, Dodd L, Kaplan R, Lacombe D, Verweij J. New response evaluation criteria in solid tumours: Revised RECIST guideline (version 1.1). Pract Radiat Oncol 2014; 45: 240-246.

[2] Heiss WD, Raab P, Lanfermann H. Multimodality Assessment of Brain Tumors and Tumor Recurrence. J Nucl Med 2011; 52: 1585-1600.

[3] Haider MA, van der Kwast TH, Tanguay J, Evans AJ, Hashmi AT, Lockwood G, Trachtenberg J. Combined T2-Weighted and Diffusion-Weighted MRI for Localization of Prostate Cancer. AJR 2007; 189: 323-328.

[4] Gatenby RA, Gillies RJ. Why do cancers have high aerobic glycolysis? Nat Rev Cancer 2004; 4: 891-899.

[5] Wahl RL, Jacene H, Kasamon Y, Lodge MA. From RECIST to PERCIST: Evolving Considerations for PET Response Criteria in Solid Tumors. J Nucl Med 2009; 50: 122S-150S.

[6] Kjær A, Loft A, Law I, Berthelsen AK, Borgwardt L, Löfgren J, Johnbeck CB, Hansen AE, Keller S, Holm S, Højgaard L. PET/MRI in cancer patients: first experiences and vision from Copenhagen. Magn Reson Mater Phy 2012; 26: 37-47.

[7] Hanahan D, Weinberg RA. Hallmarks of Cancer: The Next Generation. Cell 2011; 144: 646-674.

[8] Hansen AE, Kristensen AT, Jørgensen JT, McEvoy FJ, Busk M, van der Kogel AJ, Bussink J, Engelholm SA, Kjær A. 64Cu-ATSM and 18FDG PET uptake and 64Cu-ATSM autoradiography in spontaneous canine tumors: comparison with pimonidazole hypoxia immunohistochemistry. Radiat Oncol 2012; 7: 89.

[9] Johnbeck CB, Jensen MM, Nielsen CH, Hag AMF, Knigge U, Kjær A. 18F-FDG and 18F-FLT-PET Imaging for Monitoring Everolimus Effect on Tumor-Growth in Neuroendocrine Tumors: Studies in Human Tumor Xenografts in Mice. PLoS One 2014; 9: e91387.

[10] Vander Heiden MG, Cantley LC, Thompson CB. Understanding the Warburg Effect: The Metabolic Requirements of Cell Proliferation. Science 2009; 324: 1029-1033.
[11] Jensen MM, Erichsen KD, Johnbeck CB, Björkling F, Madsen J, Jensen PB, Sehested M, Højgaard L, Kjær A. [18F] FDG and [18F]FLT positron emission tomography imaging following treatment with belinostat in human ovary cancer xenografts in mice. BMC Cancer 2013; 13: 168.
[12] Bartrons R, Caro J. Hypoxia, glucose metabolism and the Warburg's effect. J Bioenerg Biomembr 2007; 39: 223-229.
[13] Warburg O. On the Origin of Cancer Cells. Science 1956; 123: 309-314.
[14] Cairns RA, Harris IS, Mak TW. Regulation of cancer cell metabolism. Nat Rev Cancer 2011; 11: 85-95.
[15] Binderup T, Knigge U, Loft A, Federspiel B, Kjær A. 18F-Fluorodeoxyglucose Positron Emission Tomography Predicts Survival of Patients with Neuroendocrine Tumors. Clin Cancer Res 2010; 16: 978-985.
[16] Vaupel P, Mayer A. Hypoxia in cancer: significance and impact on clinical outcome. Cancer Metastasis Rev 2007; 26: 225-239.
[17] Gambhir SS. Molecular imaging of cancer with positron emission tomography. Nat Rev Cancer 2002; 2: 683-693.
[18] Shah N, Sattar A, Benanti M, Hollander S, Cheuck L. Magnetic resonance spectroscopy as an imaging tool for cancer: a review of the literature. J Am Osteopath Assoc 2006; 106: 23-27.
[19] Ardenkjaer-Larsen JH, Fridlund B, Gram A, Hansson G, Hansson L, Lerche MH, Servin R, Thaning M, Golman K. Increase in signal-to-noise ratio of > 10,000 times in liquid-state NMR. Proc Natl Acad Sci U S A 2003; 100: 10158-10163.
[20] Brindle KM, Bohndiek SE, Gallagher FA, Kettunen MI. Tumor imaging using hyperpolarized 13C magnetic resonance spectroscopy. Magn Reson Med 2011; 66: 505-519.
[21] Day SE, Kettunen MI, Gallagher FA, Hu DE, Lerche MH, Wolber J, Golman K, Ardenkjaer-Larsen JH, Brindle KM. Detecting tumor response to treatment using hyperpolarized 13C magnetic resonance imaging and spectroscopy. Nat Med 2007; 13: 1382-1387.
[22] Brindle KM. New approaches for imaging tumour responses to treatment. Nat Rev Cancer 2008; 8: 94-107.
[23] Hansen AE, Kristensen AT, Law I, McEvoy FJ, Kjær A, Engelholm SA. Multimodality functional imaging of spontaneous canine tumors using 64 Cu-ATSM and 18 FDG PET/CT and dynamic contrast enhanced perfusion CT. Radiother Oncol 2012; 102: 424-428.
[24] Hurd RE, Yen YFF, Chen AP, Ardenkjaer-Larsen JH. Hyperpolarized 13C metabolic imaging using dissolution dynamic nuclear polarization. J Magn Reson Imaging 2012; 36: 1314-1328.
[25] Nelson SJ, Ozhinsky E, Li Y, Park I, Crane J. Strategies for rapid in vivo 1H and hyperpolarized 13C MR spectroscopic imaging. J Magn Reson 2013; 229: 187-197.
[26] Nelson SJ, Vigneron DB, Kurhanewicz J, Chen AP, Bok RA, Hurd RE. DNP-Hyperpolarized 13C Magnetic Resonance Metabolic Imaging for Cancer Applications. Appl Magn Reson 2008; 34: 533-544.
[27] Nelson SJ, Kurhanewicz J, Vigneron DB, Larson PEZ, Harzstark AL, Ferrone M, van Criekinge M, Chang JW, Bok R, Park I, Reed G, Carvajal L, Small EJ, Munster P, Weinberg VK, Ardenkjaer-Larsen JH, Chen AP, Hurd RE, Odegardstuen LI, Robb FJ, Tropp J, Murray JA. Metabolic Imaging of Patients with Prostate Cancer Using Hyperpolarized [1-13C] Pyruvate. Sci Transl Med 2013; 5: 198ra108.
[28] itney TH, Kettunen MI, Day SE, Hu DE, Neves AA, Gallagher FA, Fulton SM, Brindle KM. A comparison between radiolabeled fluorodeoxyglucose uptake and hyperpolarized (13) C-labeled pyruvate utilization as methods for detecting tumor response to treatment. Neoplasia 2009; 11: 574-582.
[29] Menzel MI, Farrell EV, Janich MA, Khegai O, Wiesinger F, Nekolla SG, Otto AM, Haase A, Schulte RF, Schwaiger M. Multimodal Assessment of In Vivo Metabolism with Hyperpolarized [1-13C] MR Spectroscopy and 18F-FDG PET Imaging in Hepatocellular Carcinoma Tumor-Bearing Rats. J Nucl Med 2013; 54: 1113-1119.